A two-dimensional fully analytical model with polarization effect for off-state channel potential and electric field distributions of GaN-based field-plated high electron mobility transistor*

Mao Wei(毛 维)[a)†], She Wei-Bo(佘伟波)[a)], Yang Cui(杨 翠)[b)], Zhang Chao(张 超)[a)], Zhang Jin-Cheng(张进成)[a)], Ma Xiao-Hua(马晓华)[b)], Zhang Jin-Feng(张金凤)[a)], Liu Hong-Xia(刘红侠)[a)], Yang Lin-An(杨林安)[a)], Zhang Kai(张 凯)[a)], Zhao Sheng-Lei(赵胜雷)[a)], Chen Yong-He(陈永和)[a)], Zheng Xue-Feng(郑雪峰)[a)], and Hao Yue(郝 跃)[a)]

[a)] *Key Laboratory of Ministry of Education for Wide Band-Gap Semiconductor Materials and Devices, School of Microelectronics, Xidian University, Xi'an* 710071, *China*

[b)] *School of Physics and Optoelectronic Engineering, Xidian University, Xi'an* 710071, *China*

(Received 8 October 2013; revised manuscript received 24 November 2013; published online 10 June 2014)

In this paper, we present a two-dimensional (2D) fully analytical model with consideration of polarization effect for the channel potential and electric field distributions of the gate field-plated high electron mobility transistor (FP-HEMT) on the basis of 2D Poisson's solution. The dependences of the channel potential and electric field distributions on drain bias, polarization charge density, FP structure parameters, AlGaN/GaN material parameters, etc. are investigated. A simple and convenient approach to designing high breakdown voltage FP-HEMTs is also proposed. The validity of this model is demonstrated by comparison with the numerical simulations with Silvaco–Atlas. The method in this paper can be extended to the development of other analytical models for different device structures, such as MIS-HEMTs, multiple-FP HETMs, slant-FP HEMTs, etc.

Keywords: analytical model of GaN-based field-plated HEMT, polarization effect, potential, electric field

PACS: 73.40.Kp, 85.30.Tv, 85.30.De **DOI:** 10.1088/1674-1056/23/8/087305

1. Introduction

Field-plate (FP) technologies, with their origins in the context of high-voltage p–n junctions,[1] have been one of the most important catalysts for improving the microwave power performances of GaN-based high electron mobility transistors (HEMTs).[2–4] These techniques could be effective in extending the drain depletion region and replacing a single-peak electric field with several peaks[5] by modulating the potential distribution along the device channel, which could bring into uniformity the electric field distribution and improve device, breakdown performance, and other relevant reliability performance, such as trapping effect,[6–8] inverse piezoelectric effect,[9,10] etc. Therefore, the effect of the FP on the electric field distribution related to the potential distribution is a key factor for the GaN-based FP-HEMT with high breakdown voltage and excellent reliability. In recent years, many groups have paid much attention to FP-HEMTs by means of experimental device fabrications, which could not directly reveal the inherent mechanism of the FP modulation associated with device structure parameters such as FP structure parameters, semiconductor material parameters, etc. Analytical approach is an important and effective way to gain a physical insight into the essential mechanism of the modulation of the FP, which could also shorten the design cycle and simplify the optimization procedure by providing fast and accurate first-order design schemes compared with numerical simulations. In 2005, Karmalkar *et al.* first proposed an analytical approach for a GaN-based FP-HEMT with a given drain bias[11] and they further modeled the dependence of the channel field distribution on drain bias in 2006.[12] These models had some guiding signification for the FP-HEMT design, while they were based on the curve fitting of the numerical simulation profiles rather than analytical solution of Poisson equation. There exist some challenges for them in more complex device structures, such as multiple-FP HETMs,[5,13] slant-FP HEMTs,[14,15] etc. Furthermore, in these models the potential distribution was not investigated. In 2007 Kumar *et al.* reported on a threshold voltage model for small geometry AlGaN/GaN HEMTs without FP based on analytical solution of Poisson equation[16] and they also reported on two analytical models of the nanoscale dual material gate AlGaN/GaN HEMTs without FP in 2008.[17,18] These analytical models could be successful at predicting the channel potential and electric field distributions for small geometry HEMTs, while they did not include the polarization effect and only hold for very small drain bias. So far, no analytical model completely based on Poisson solution with consideration of the polariza-

*Project supported by the National Natural Science Foundation of China (Grant Nos. 61204085 and 61334002) and the Fundamental Research Funds for the Central Universities, China (Grant No. K5051225013).

†Corresponding author. E-mail: mwxidian@126.com

© 2014 Chinese Physical Society and IOP Publishing Ltd

tion effect has been developed to investigate the channel potential and electric field distributions of the GaN-based FP-HEMT under high drain bias, which deserves to be investigated further.

In this paper, for the first time, a two-dimensional (2D) fully analytical model with consideration of polarization effect for the channel potential and electric field distributions of the gate FP-HEMT in terms of Poisson solution is presented. The lateral spread of the depletion region between the FP and the drain is also considered. The dependences of the channel potential and electric field on drain bias and several parameters in the FP-HEMT are discussed in detail. The analytical results of the proposed models show a good agreement with the numerical simulation results obtained by Silvaco-atlas.[19]

2. Model formulation

2.1. Considerations for modeling

The schematic cross section of the gate FP-HEMT with SiN passivation layer is shown in Fig. 1(a), where x measures the horizontal position relative to the left edge of the gate while y measures the vertical position relative to the AlGaN layer surface. This structure is similar to that used in Refs. [11] and [20]. In Fig. 1(a), d_3 and ε_3 denote respectively the thickness and the dielectric constant of the passivation layer, d_1 and d_2 the thickness values of the AlGaN layer and GaN layer, ε_1 and ε_2 the dielectric constants of the AlGaN layer and the GaN layer, N_1 and N_2 the donor doping concentration of the AlGaN layer and the background donor concentration of the GaN layer, L_1 and L_2 the length of the gate and the effective length of the FP, and L_3 is the distance from the drain side of the FP to drain (FP-drain spacing). The positive charge is located along the AlGaN/GaN heterojunction to model the polarization effect, which is based on the experimental result of the approximate charge neutrality at the AlGaN/passivation layer interface.[21] In Fig. 1(a), σ_p denotes the polarization sheet charge density, x_{Al} the aluminum content of the AlGaN barrier layer, the source–gate and the source–drain spacings are 0.5 μm and 3.5 μm respectively (unless otherwise stated), the source (S) is grounded, and V_{GS} and V_{DS} are the biases of the gate and drain respectively. In the following discussion, V_{GS} is biased to -10 V, in which case the FP-HEMT is fully pinched off. In Fig. 1(a), the whole region of the AlGaN layer and the GaN layer from the left edge of the gate (G) to the drain (D) is divided into six regions named as I, II, III, IV, V, and VI, and their boundary positions are given by $x = 0$, L_1, $L_1 + L_2$, $L_1 + L_2 + L_3$, and $y = 0$, d_1, $d_1 + d_2$.

The electron concentration profile in the FP-HEMT with 0.1-μm SiN passivation layer and 1-μm FP at $V_{GS} = -10$ V and $V_{DS} = 250$ V is numerically simulated, and the result is shown in Fig. 1(b). The device is pinched off. From Fig. 1(b) one could observe that the depletion regions in the AlGaN

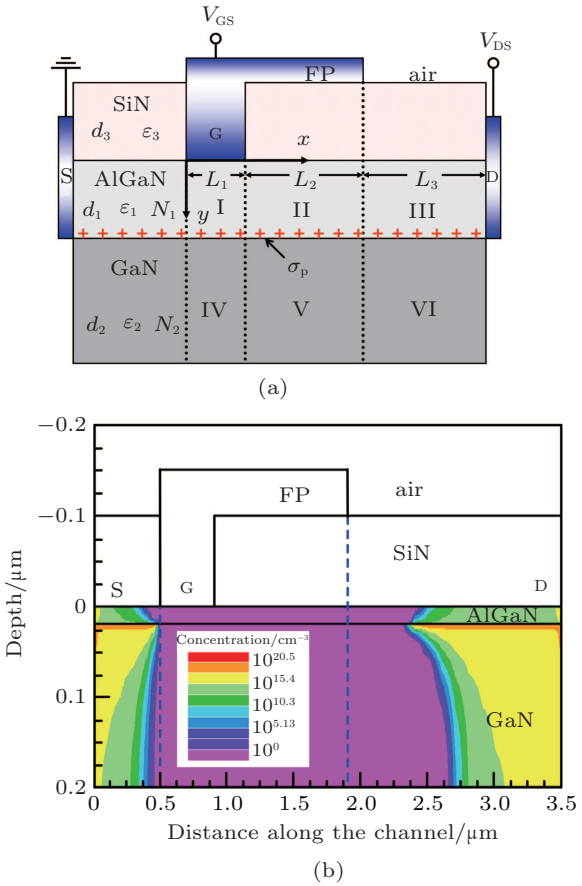


Fig. 1. (color online) (a) Schematic cross section of the gate FP-HEMT and (b) electron concentration profile in the FP-HEMT with 0.1-μm SiN passivation layer and 1-μm FP at $V_{GS} = -10$ V and $V_{DS} = 250$ V.

layer and the GaN layer are distributed from the source side near the gate to the drain. Based on our simulation results and others reported,[5,20] the important regions, with which we are concerned in this paper, are those that are just under the gate and the FP in semiconductor because the maximum electric field often exists here. And the breakdown voltage of the FP-HEMT is determined by the electric field distribution and the electric field peak in this region to a great extent.[20] Usually, the electric field and the potential in the region above could be influenced by the depletion region between the drain side of the FP and the drain. However, due to the complexity, it is difficult to accurately calculate the lateral spread of the depletion region between the drain side of the FP and the drain. Fortunately, careful observation shows that the actual depletion region in an FP-HEMT at a drain bias of V_{DS} could be considered as the combination of the depletion regions under two kinds of assumptions. The first assumption is that the full region in the semiconductors between the source side of the gate and the drain are depleted. The second assumption is that the depletion region is distributed only under the gate and the FP. Under the second assumption, there exists enough two-dimensional (2D) electron gas along the AlGaN/GaN heterostructure channel between the drain side of the FP and the drain. Thus, the access resistance along the channel between the drain side of the FP and the drain is so small that it could

be neglected and we could assume that the drain voltage V_{DS} is directly applied to the point on the drain side of the FP in the channel. Although the depletion region could also extend from the source side of the gate towards the source in Fig. 1(b), its area is very small and could be neglected so as to focus on the key points. Due to the vertical electric field being small in the resultant electric field, the lateral electric field could be used to represent the total resultant electric field for simplicity.[11,12] Thus our studies of the electric field focuses on the lateral electric field along the channel which can be directly related to the drain voltage V_{DS}.

2.2. 2D potential and electric field analyses

For the sake of analysis, six different 2D potential functions are introduced to describe the potential distribution in six regions shown in Fig. 1(a). They are $\varphi_1(x,y)$ (in region I for $0 \le x \le L_1$, $0 \le y \le d_1$), $\varphi_2(x,y)$ (in region II for $L_1 \le x \le L_1+L_2$, $0 \le y \le d_1$), $\varphi_3(x,y)$ (in region III for $L_1+L_2 \le x \le L_1+L_2+L_3$, $0 \le y \le d_1$), $\varphi_4(x,y)$ (in region IV for $0 \le x \le L_1$, $d_1 \le y \le d_1+d_2$), $\varphi_5(x,y)$ (in region V for $L_1 \le x \le L_1+L_2$, $d_1 \le y \le d_1+d_2$), and $\varphi_6(x,y)$ (in region VI for $L_1+L_2 \le x \le L_1+L_2+L_3$, $d_1 \le y \le d_1+d_2$). Under the first assumption, all the six regions are fully depleted under the off-state condition of $V_{GS} = -10$ V. These potential functions in their corresponding regions must satisfy the 2D Poisson equation, thus yielding

$$\frac{\partial^2 \varphi_i(x,y)}{\partial x^2} + \frac{\partial^2 \varphi_i(x,y)}{\partial y^2} = -\frac{qN_1}{\varepsilon_1}, \quad i = 1,2,3, \tag{1a}$$

$$\frac{\partial^2 \varphi_i(x,y)}{\partial x^2} + \frac{\partial^2 \varphi_i(x,y)}{\partial y^2} = -\frac{qN_2}{\varepsilon_2}, \quad i = 4,5,6, \tag{1b}$$

where q is the electronic charge, $\varepsilon_1 = \varepsilon_0\varepsilon_{r1}$, $\varepsilon_2 = \varepsilon_0\varepsilon_{r2}$, with ε_{r1} and ε_{r2} being the relative dielectric constant of the AlGaN layer and the GaN layer, and ε_0 the vacuum permittivity. And the potential function $\varphi_i(x,y)$ (i = 1, 2, 3, 4, 5, 6) in the vertical direction can be approximated by a simple parabolic function[17,18]

$$\varphi_i(x,y) = \varphi_i(x) + C_{1i}(x)(y-d_1) + C_{2i}(x)(y-d_1)^2, \quad i = 1,2,3,4,5,6, \tag{2}$$

where $\varphi_i(x)$ is the AlGaN/GaN heterostructure channel potential for each region and $C_{1i}(x)$ and $C_{2i}(x)$ are the arbitrary coefficients. The Poisson equations (1a) and (1b) are solved using the following boundary conditions.

1) Potentials at the source end and drain end are

$$\varphi_1(0,d_1) = 0, \tag{3}$$

$$\varphi_3(L,d_1) = V_{DS}, \tag{4}$$

where $L = L_1+L_2+L_3$. For simplicity, the built-in potential V_{bi} is neglected in Eqs. (3) and (4) since it is much smaller than the applied voltage V_{DS}.

2) Electric field at the bottom of GaN layer may be minimized as

$$\left.\frac{\partial \varphi_i(x,y)}{\partial y}\right|_{y=d_1+d_2} = 0, \quad i = 4,5,6, \tag{5}$$

which is due to the fact that the thickness of GaN layer d_2 is large enough, such as $d_2 = 0.18$ μm.

3) Electric displacement at the interface between the passivation layer and the AlGaN layer is continuous

$$\varepsilon_1 \left.\frac{\partial \varphi_2(x,y)}{\partial y}\right|_{y=0} = \varepsilon_3 \frac{\varphi_2(x,0) - V_{GS}}{d_3}, \tag{6}$$

$$\varepsilon_1 \left.\frac{\partial \varphi_3(x,y)}{\partial y}\right|_{y=0} = \varepsilon_3 \frac{\varphi_3(x,0) - V_f}{d_3}, \tag{7}$$

where $\varepsilon_3 = \varepsilon_0\varepsilon_{r3}$, ε_{r3} being the relative dielectric constant of the passivation layer, $V_f = (V_{DS} - V_{GS})(x-l)/L_3 + V_{GS}$ is the linear potential at the interface between the passivation layer and the air from the drain side of the FP to the drain on the assumption that the electric field along the passivation layer surface may be minimized.[22]

4) Electric displacement at the AlGaN/GaN interface is continuous, so

$$\varepsilon_1 \left.\frac{\partial \varphi_1(x,y)}{\partial y}\right|_{y=d_1} - \varepsilon_2 \left.\frac{\partial \varphi_4(x,y)}{\partial y}\right|_{y=d_1} = q\sigma_p, \tag{8}$$

$$\varepsilon_1 \left.\frac{\partial \varphi_2(x,y)}{\partial y}\right|_{y=d_1} - \varepsilon_2 \left.\frac{\partial \varphi_5(x,y)}{\partial y}\right|_{y=d_1} = q\sigma_p, \tag{9}$$

$$\varepsilon_1 \left.\frac{\partial \varphi_3(x,y)}{\partial y}\right|_{y=d_1} - \varepsilon_2 \left.\frac{\partial \varphi_6(x,y)}{\partial y}\right|_{y=d_1} = q\sigma_p. \tag{10}$$

5) Potential at the interface between the gate and the AlGaN layer is

$$\varphi_1(x,0) = V_{GS} - V_{FB} = V_g, \tag{11}$$

where $V_{FB} = \Phi_{MS} = \Phi_M(\mathrm{Ni}) - \Phi_S(x_{Al}) = \Phi_B(x_{Al}) - \Phi_n$ is the flat-band voltage, $\Phi_M(\mathrm{Ni})$ and $\Phi_S(x_{Al})$ are the work functions of the gate metal Ni and the AlGaN layer with the aluminum content x_{Al}, $\Phi_B(x_{Al})$ is the Schottky barrier height of Ni/AlGaN,[23] $\Phi_n = (kT/q)\ln(N_c/N_1)$, k is the Boltzmann constant, N_c is the effective density of states in conduction band in AlGaN layer and $T = 300$ K.

6) Potentials and electric fields at the AlGaN/GaN interface are continuous, so

$$\varphi_1(x,d_1) = \varphi_4(x,d_1), \tag{12}$$

$$\varphi_2(x,d_1) = \varphi_5(x,d_1), \tag{13}$$

$$\varphi_3(x,d_1) = \varphi_6(x,d_1), \tag{14}$$

$$\varphi_1(L_1,d_1) = \varphi_2(L_1,d_1), \tag{15}$$

$$\varphi_2(l,d_1) = \varphi_3(l,d_1) = V'_{DS}, \tag{16}$$

$$\left.\frac{\partial \varphi_1(x,y)}{\partial x}\right|_{x=L_1,y=d_1} = \left.\frac{\partial \varphi_2(x,y)}{\partial x}\right|_{x=L_1,y=d_1}, \tag{17}$$

$$\left.\frac{\partial \varphi_2(x,y)}{\partial x}\right|_{x=l,y=d_1} = \left.\frac{\partial \varphi_3(x,y)}{\partial x}\right|_{x=l,y=d_1}, \tag{18}$$

where $l = L_1 + L_2$.

The σ_p is a function of the aluminum content x_{Al} of the $Al_{x_{Al}}Ga_{1-x_{Al}}N$ barrier layer. Based on the polarization theories,[24] σ_p at the AlGaN/GaN interface due to the piezoelectric and spontaneous polarization is given by

$$\sigma_p(x_{Al}) = |P_{PE}(Al_{x_{Al}}Ga_{1-x_{Al}}N) + P_{SP}(Al_{x_{Al}}Ga_{1-x_{Al}}N) - P_{SP}(GaN)|, \quad (19)$$

where

$$P_{SP}(Al_{x_{Al}}Ga_{1-x_{Al}}N) - P_{SP}(GaN) = -0.052x_{Al} \quad (20)$$

is the interface charge due to the spontaneous polarization at AlGaN/GaN heterostructure. And

$$P_{PE}(Al_{x_{Al}}Ga_{1-x_{Al}}N) = 2[1-r(x_{Al})]\frac{a_{GaN}-a_{AlGaN}(x_{Al})}{a_{AlGaN}(x_{Al})} \times \left[e_{31}(x_{Al}) - e_{33}(x_{Al})\frac{C_{13}(x_{Al})}{C_{33}(x_{Al})}\right] \quad (21)$$

is the interface charge due to the variation of the strain-induced piezoelectric polarization at AlGaN/GaN heterostructure. In Eq. (21), $r(x_{Al})$ is the degree of strain relaxation of the $Al_{x_{Al}}Ga_{1-x_{Al}}N$ layer; a_{GaN} and $a_{AlGaN}(x_{Al})$ are the crystal lattice constants for GaN and $Al_{x_{Al}}Ga_{1-x_{Al}}N$, respectively; $C_{13}(x_{Al})$ and $C_{33}(x_{Al})$ are the elastic constants; $e_{31}(x_{Al})$ and $e_{33}(x_{Al})$ are the piezoelectric constants. Linear interpolations between the physical properties of GaN and AlN are used to calculate the above parameters of $Al_{x_{Al}}Ga_{1-x_{Al}}N$. All the parameters in Eqs. (19)–(21) can be found in Ref. [25]. Table 1 shows the values of polarization sheet charge density σ_p at different values of aluminum content x_{Al} of AlGaN barrier layer according to Eq. (19).

Table 1. Values of polarization sheet charge density σ_p at different values of aluminum content x_{Al} of AlGaN barrier layer.

x_{Al}	σ_p/cm^{-2}
0.2	1.06×10^{13}
0.3	1.64×10^{13}
0.4	2.18×10^{13}
0.5	2.40×10^{13}

Substituting Eq. (2) into Eqs. (1a) and (1b) yields

$$\frac{d^2\phi_i(x)}{dx^2} + 2C_{2i}(x) = -\frac{qN_1}{\varepsilon_1}, \quad i = 1,2,3, \quad (22a)$$

$$\frac{d^2\phi_i(x)}{dx^2} + 2C_{2i}(x) = -\frac{qN_2}{\varepsilon_2}, \quad i = 4,5,6. \quad (22b)$$

According to the boundary conditions (5)–(14), the coefficient $C_{2i}(x)$ ($i = 1, 2, 3, 4, 5, 6$) could be represented by $\phi_i(x)$ and equations (22a) and (22b) could be simplified into

$$\frac{d^2\phi_i(x)}{dx^2} - \alpha_i\phi_i(x) = \beta_i, \quad i = 1,2, \quad (23a)$$

$$\frac{d^2\phi_3(x)}{dx^2} - \alpha_2\phi_3(x) = \beta_3 + \gamma x, \quad (23b)$$

where

$$\alpha_1 = \left[\frac{\varepsilon_2 d_1 d_2}{\varepsilon_1} + \frac{d_1^2}{2}\right]^{-1},$$

$$\alpha_2 = \left[\frac{\varepsilon_2 d_2 d_3}{\varepsilon_3} + \frac{\varepsilon_1 d_1 d_3}{\varepsilon_3} + \frac{\varepsilon_2 d_1 d_2}{\varepsilon_1} + \frac{d_1^2}{2}\right]^{-1},$$

$$\beta_1 = \frac{q\sigma_p}{\varepsilon_2 d_2} - \frac{qN_2}{\varepsilon_2} + \frac{\alpha_1}{2}\left[\left(\frac{qN_2}{\varepsilon_2} - \frac{qN_1}{\varepsilon_1} - \frac{q\sigma_p}{\varepsilon_2 d_2}\right)d_1^2 - 2V_g\right],$$

$$\beta_2 = \frac{q\sigma_p}{\varepsilon_2 d_2} - \frac{qN_2}{\varepsilon_2} + \frac{\alpha_2}{2}\left[\left(\frac{qN_2}{\varepsilon_2} - \frac{qN_1}{\varepsilon_1} - \frac{q\sigma_p}{\varepsilon_2 d_2}\right) \times \left(\frac{2\varepsilon_1 d_1 d_3}{\varepsilon_3} + d_1^2\right) - 2V_{GS}\right],$$

$$\beta_3 = -\frac{qN_1}{\varepsilon_1} - \alpha_2\left[\left(\frac{qN_2}{\varepsilon_2} - \frac{qN_1}{\varepsilon_1} - \frac{q\sigma_p}{\varepsilon_2 d_2}\right) \times \left(\frac{\varepsilon_2 d_2 d_3}{\varepsilon_3} + \frac{\varepsilon_2 d_1 d_2}{\varepsilon_1}\right) + V_{GS} - \frac{V_{DS}-V_{GS}}{L_3}l\right],$$

$$\gamma = -\frac{V_{DS}-V_{GS}}{L_3}\alpha_2.$$

Equations (23a) and (23b) are the second-order differential equations and the expression for the AlGaN/GaN heterostructure channel potential is in the following form:

$$\phi_C = \begin{cases} \phi_1(x) = A_1\exp(\eta_1 x) + B_1\exp(-\eta_1 x) - \xi_1, \\ \qquad 0 \le x \le L_1, \\ \phi_2(x) = A_2\exp(\eta_2 x) + B_2\exp(-\eta_2 x) - \xi_2, \\ \qquad L_1 \le x \le l, \end{cases} \quad (24a)$$

$$\phi_3(x) = A_3\exp(\eta_2 x) + B_3\exp(-\eta_2 x) - \xi_3 - \xi_4 x, \quad l \le x \le L. \quad (24b)$$

Here, A_i and B_i ($i = 1,2,3$) are the coefficients, $\eta_1 = \sqrt{\alpha_1}$, $\eta_2 = \sqrt{\alpha_2}$, $\xi_1 = \beta_1/\alpha_1$, $\xi_2 = \beta_2/\alpha_2$, $\xi_3 = \beta_3/\alpha_2$, $\xi_4 = \gamma/\alpha_2$, ϕ_C is the channel potential under the gate and the FP, $\phi_3(x)$ is the channel potential between the drain side of the FP and the drain under the assumption of full depletion in the region III and the region VI.

According to our assumption above, the actual depletion region could be considered as the combination of two kinds of depletion regions, which leads to two kinds of channel potential distributions correspondingly. Let ϕ_{C1} be defined as the channel potential under the gate and the FP corresponding to the first assumption and φ_{C2} the one corresponding to the second assumption. Thus the channel potential distribution in an FP-HEMT could be calculated to be a combination of ϕ_{C1} and ϕ_{C2}.

According to the derivative process mentioned above under the first assumption, the channel potential ϕ_{C1} can be obtained. And the coefficients A_i and B_i ($i = 1, 2, 3$) can be obtained by solving Eqs. (20) and (21) with the boundary conditions of Eqs. (3), (4), and (15)–(17) as

$$A_1 = \{\xi_1[\theta_1\exp(\eta_2 L_2 - \eta_1 L_1) - \theta_2\exp(-\eta_2 L_2 - \eta_1 L_1)]$$

$$+\theta_3(\xi_1-\xi_2)[\exp(\eta_2 L_2)+\exp(-\eta_2 L_2)] + 2\theta_3(V'_{DS}+\xi_2)\}/\lambda_1, \quad (25a)$$

$$B_1 = \{-\xi_1[\theta_1\exp(-\eta_2 L_2+\eta_1 L_1)-\theta_2\exp(\eta_2 L_2+\eta_1 L_1)] - \theta_3(\xi_1-\xi_2)[\exp(\eta_2 L_2)+\exp(-\eta_2 L_2)] - 2\theta_3(V'_{DS}+\xi_2)\}/\lambda_1, \quad (25b)$$

$$A_2 = \{-2\xi_1\exp(-\eta_2 l)+(\xi_1-\xi_2)[\exp(\eta_1 L_1-\eta_2 l) + \exp(-\eta_1 L_1-\eta_2 l)]+[\theta_1\exp(-\eta_2 L_1-\eta_1 L_1) + \theta_2\exp(-\eta_2 L_1+\eta_1 L_1)](V'_{DS}+\xi_2)\}/\lambda_1, \quad (25c)$$

$$B_2 = \{2\xi_1\exp(\eta_2 l)-(\xi_1-\xi_2)[\exp(\eta_1 L_1+\eta_2 l) + \exp(-\eta_1 L_1+\eta_2 l)]-[\theta_1\exp(\eta_2 L_1+\eta_1 L_1) + \theta_2\exp(\eta_2 L_1-\eta_1 L_1)](V'_{DS}+\xi_2)\}/\lambda_1, \quad (25d)$$

$$A_3 = [(V_{DS}+\xi_3+\xi_4 L)\exp(-\eta_2 l)-(V'_{DS}+\xi_3+\xi_4 l) \times \exp(-\eta_2 L)]/\lambda_2, \quad (25e)$$

$$B_3 = [-(V_{DS}+\xi_3+\xi_4 L)\exp(\eta_2 l)+(V'_{DS}+\xi_3+\xi_4 l) \times \exp(\eta_2 L)]/\lambda_2, \quad (25f)$$

where

$$\lambda_1 = \theta_1\{\exp(\eta_2 L_2-\eta_1 L_1)-\exp[-(\eta_2 L_2-\eta_1 L_1)]\} + \theta_2\{\exp(\eta_2 L_2+\eta_1 L_1)-\exp[-(\eta_2 L_2+\eta_1 L_1)]\},$$

$$\lambda_2 = \exp(\eta_2 L_3)-\exp(-\eta_2 L_3).$$

Since the electric field are continuous at the interfaces of the region II and the region III as indicated in Eq. (18), the expression of the V'_{DS} can be obtained as

$$V'_{DS} = \left\{\begin{array}{l}\lambda_1\{2(V_{DS}+\xi_3+\xi_4 L)-(\xi_3+\xi_4 l)[\exp(\eta_2 L_3) \\ +\exp(-\eta_2 L_3)]+\lambda_2\theta_4\}+\lambda_2\{4\xi_1 \\ -2(\xi_1-\xi_2)[\exp(\eta_1 L_1)+\exp(-\eta_1 L_1)] \\ -\xi_2[\lambda_1+2\theta_1\exp(-\eta_2 L_2+\eta_1 L_1) \\ +2\theta_2\exp(-\eta_2 L_2-\eta_1 L_1)]\}\end{array}\right\}/\lambda_3,$$

where

$$\lambda_3 = 2\theta_1\{\exp[\eta_2(L_2+L_3)-\eta_1 L_1] - \exp[-\eta_2(L_2+L_3)+\eta_1 L_1]\} + 2\theta_2\{\exp[\eta_2(L_2+L_3)+\eta_1 L_1] - \exp[-\eta_2(L_2+L_3)-\eta_1 L_1]\}.$$

Hence the channel potential ϕ_{C1} is given by

$$\phi_{C1} = \left\{\begin{array}{l}\phi_1(x) = A_1\exp(\eta_1 x)+B_1\exp(-\eta_1 x)-\xi_1, \\ \quad 0 \le x \le L_1, \\ \phi_2(x) = A_2\exp(\eta_2 x)+B_2\exp(-\eta_2 x)-\xi_2, \\ \quad L_1 \le x \le l.\end{array}\right. \quad (26)$$

Under the second assumption, the regions III and VI could not be considered and the channel potential ϕ_{C2} can be obtained with a similar approach to ϕ_{C1}. The coefficients A_i and B_i ($i = 1, 2$) can be obtained by solving Eq. (24a) with the boundary conditions of Eqs. (3) and (15)–(17). The expressions of ϕ_{C2} are the same as those in Eq. (26), respectively, and the expressions of coefficients A_i and B_i ($i = 1, 2$) are the same as Eqs. (25a)–(25d) except that V'_{DS} in these equations is replaced by V_{DS}.

Therefore, the final expression for the channel potential under the gate and the FP can be obtained by the combination of ϕ_{C1} and ϕ_{C2} as

$$\phi_{C,f} = \omega\phi_{C1}+(1-\omega)\phi_{C2}, \quad (27)$$

where ω is the weighting factor. Because at any drain bias there exists the lateral spread of the depletion region, ω is determined to be 0.7 so as to stress the contribution of the lateral spread, in which case the results obtained by our analytical model accord well with those obtained by the numerical simulation. It is worth mentioning that ω may be a variable of the drain bias and the device parameter, which is of significance and of great use and is our future goal and work. Correspondingly, the electric field along the channel could be obtained by differentiating Eq. (27) with respect to x. For convenience, the absolute value of the lateral electric field is adopted in the following.

3. Results and discussion

Based on the above analytical model (27), the potential and the lateral electric field distributions along the AlGaN/GaN heterostructure channel could be readily obtained. In order to verify the proposed model, the 2D device numerical simulation is performed using Silvaco–Atlas for the same structure. In the following discussion, the curves denote the analytical results while the symbol-points represent the numerical results. And all the conditions related to the discussion are listed in the corresponding figures.

Figure 2 shows the channel potential and channel lateral electric field distributions for different values of SiN passivation thickness d_3. A fair accordance between the analytical and the numerical results could be found except a few small discrepancies. These discrepancies around the source side of the gate edge and around the drain side of the gate edge are attributed to the neglecting of the depletion region between the source and the gate and to the neglecting of the fringe field of the gate in our analytical model respectively. And the discrepancies around the drain side of the FP are attributed to the constant estimation of the depletion region between the drain edge of the FP and the drain. As it can be seen, with the increase of d_3, the channel potential near the drain side of the FP rises slowly, while that near the gate edge of the FP goes up faster, which indicates the highest electric field peak may

move from the drain side of the FP to the drain side of the gate edge, correspondingly. Those may lead to not only the increase of gate leakage current and the deterioration of reliability but also the change of the maximum breakdown point due to the GaN breakdown field of 3 MV/cm. And the maximum breakdown voltage can be obtained when the two electric field peaks, around the drain side of the gate edge and around the drain side of the FP, each has a uniform value of less than 3 MV/cm, such as in the case of d_3 of about 0.185-μm. This indicates that the 0.185-μm SiN passivaton layer is approximately an optimum choice to achieve a breakdown voltage of $V_{DS} = 250$ V, resulting in a maximum operating bias of about 125 V for device. A similar FP-HEMT with 0.2-μm SiN layer and 1.1-μm FP in Ref. [3] could be biased at 120 V, which is quite close to our optimum result.

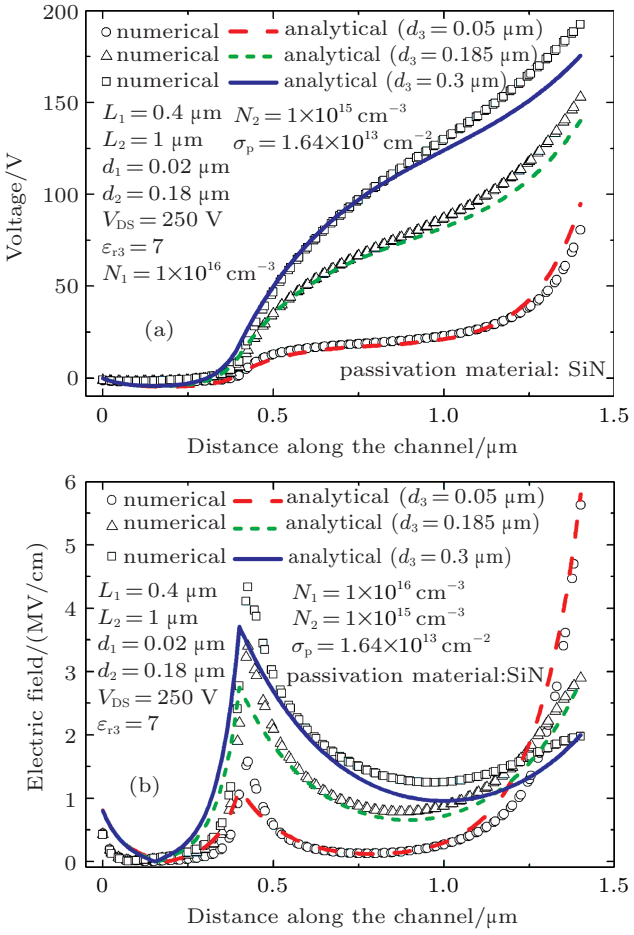


Fig. 2. (color online) (a) Channel potential and (b) lateral electric field distributions of the FP-HEMT for different values of SiN passivation thickness d_3.

Figure 3 shows the influences of the different values of FP length L_2 with the channel potential. As it can be seen, with the increase of L_2, both the potentials near the drain side of the gate and those near the drain side of the FP change slightly, while the variation of the potential under the FP becomes slower. These indicate the slight changes of the electric field peaks near the two sides and the smaller electric field under the FP.

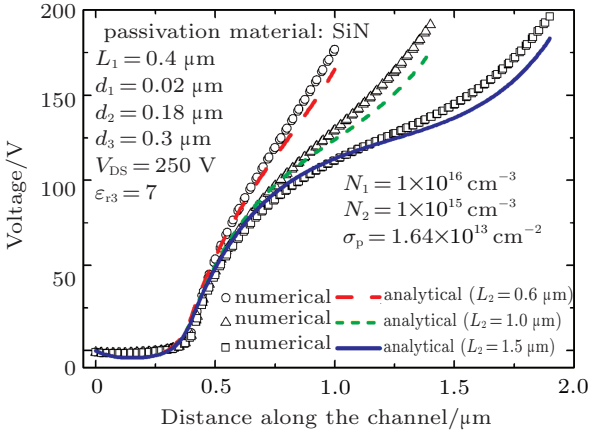


Fig. 3. (color online) Channel potential distributions for different values of FP length L_2.

The dependences of the channel potential on drain–source voltage V_{DS} are shown in Fig. 4. When other parameters are fixed, with the increase of V_{DS}, the channel potential near the drain side of the FP increases gradually, while that near the gate almost remains unchanged. These results indicate that the increment of V_{DS} is mostly applied to the region nearby drain side of the FP edge. Thus, the FP can be regarded as a clamper, and it could nearly pin the variation of the channel potential near the gate and the potential drop across the region at gate edge. Correspondingly, it could be predicted from those observations that only the electric field near the drain side of the FP could continue to increase with the increase of V_{DS}.

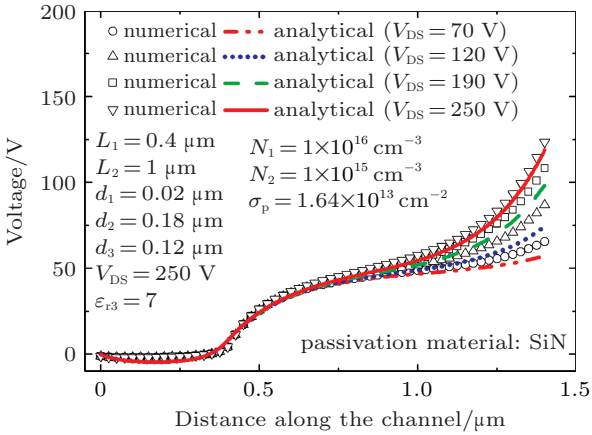


Fig. 4. (color online) Channel potential distributions for different values of drain–source voltage V_{DS}.

The passivation material could also influence the modulation effect of the FP on channel potential and electric field distributions as shown in Fig. 5. In Fig. 5, SiN, Al_2O_3, and $HfSiO_4$, whose relative dielectric constant (ε_{r3}) values are 7, 9, and 12, respectively, are utilized as the passivation materials. As it can be seen, with the increase of ε_{r3}, the variation rate of the potential near the gate edge of the FP becomes smaller, while that near the drain side of FP hardly changes, which results in a smaller electric field peak near the gate side and an almost constant electric field peak near the drain side.

According to this analysis here and the results in Fig. 4, one could gain enlightenment that the adoption of the passivation material with a proper high ε_{r3} is helpful for the FP to further modulate the channel electric field and improve the device breakdown voltage. This conclusion is consistent with that in Ref. [20] and could be well verified by our previous experimental studies[26] about the FP-HEMT with HfO_2 passivation material by means of device fabrication.

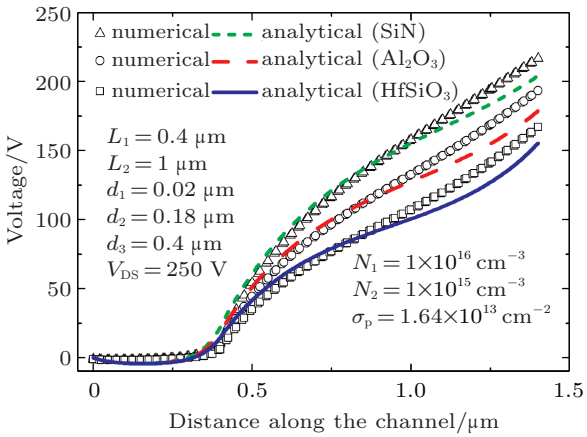


Fig. 5. (color online) Channel potential distributions for different passivation materials.

Figure 6 shows the channel potential distributions for different values of polarization sheet charge density σ_p. As it can be seen, with the increase of σ_p, the variation rate of the potential near the drain side of the gate becomes greater while it becomes insensitive to σ_p at high aluminum content, which shows a gradual increase in electric field peak. And the variation rate of the potential near the drain side of FP hardly changes, indicating little changes of the electric field here.

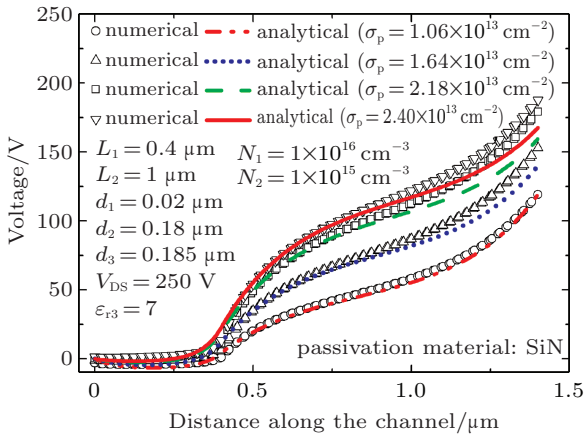


Fig. 6. (color online) Channel potential distributions for different values of polarization sheet charge density σ_p.

Figure 7 shows the influence of the doping concentration N_1 of the AlGaN barrier layer on channel potential distribution. From Fig. 7, one could find it is very interesting that the effect of N_1 is similar to that of the polarization sheet charge density expect that the effect near the source side of the gate is smaller and the effect near the drain side of the FP becomes slightly greater. These results show that more electric field lines generated from the ionized donor dopant could terminate in the region near the drain side of the gate for the FP-HEMT with the increase of the doping concentration in the AlGaN barrier layer, which is also demonstrated in Ref. [27]. Thus, the reduction of AlGaN layer doping concentration is effective in the high breakdown voltage design. And for the FP-HEMT with heavy doping concentration in AlGaN layer, it is necessary to adjust other parameters, such as passivation thickness or relative dielectric constant of the passivation layer, to avoid the peak electric field near the gate exceeding the breakdown field.

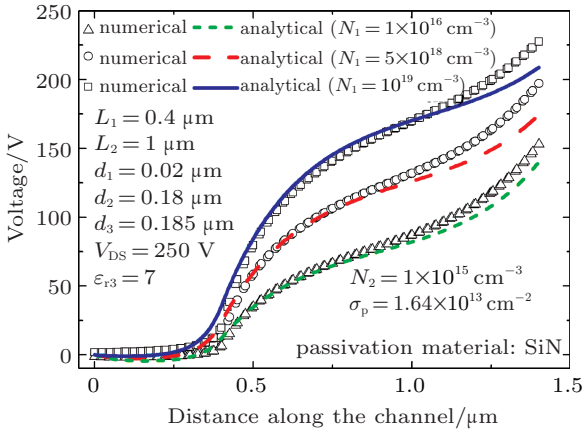


Fig. 7. (color online) Channel potential distributions for different values of doping concentration N_1 of the AlGaN barrier layer.

The influences of the background concentration N_2 of the GaN buffer layer on channel potential for the FP-HEMT are shown in Fig. 8. Obviously, the influence of the background concentration is also similar to that of the polarization sheet charge density in Fig. 6 except that the influence is smaller. From these observations, in order to avoid breakdown it is needed to slightly adjust the FP structure parameters to lower the peak electric field near the gate edge. Actually, heavy background concentration could also lead to great buffer leakage, which may severely degrade the breakdown performance.[28] Therefore, solutions to the suppression of buffer leakage should also be considered for the design of the FP-HEMT with heavy background concentration.

In addition, the dependence of the channel potential distribution on active efficiency of donor in the AlGaN barrier layer or the GaN buffer layer is similar to that of N_1 or N_2. The study results of other parameters, such as AlGaN layer thickness d_1, GaN layer thickness d_2, gate length L_1, and FP-drain spacing L_3 show that they each have a weak effect on the channel potential and electric field distributions.

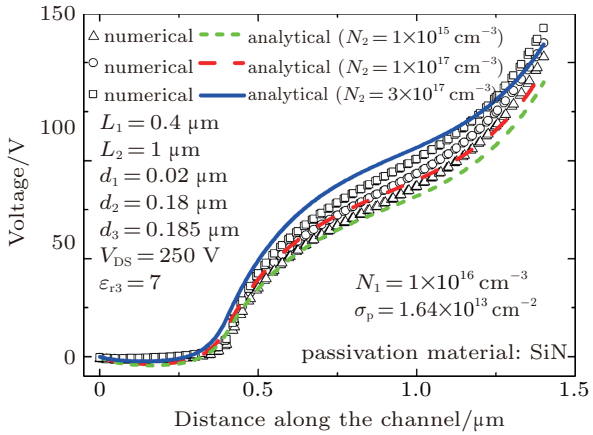


Fig. 8. (color online) Channel potential distributions for different values of background concentration N_2 of the GaN buffer layer.

From the above discussion, in order to gain the maximum breakdown voltage, a necessary condition that the electric field peaks on the drain side of the gate edge $E_{C,f}(L_1)$ and that on the drain side of the FP edge $E_{C,f}(l)$ each should have a uniform value which could not be larger than the GaN critical value of $E_c = 3$ MV/cm, should be satisfied. In other words, the following inequality holds:

$$E_{C,f}(L_1) = E_{C,f}(l) \leq E_c. \tag{28}$$

Based on Eq. (28), it is convenient to design an FP-HEMT with a highest breakdown voltage available by optimizing these parameters mentioned above.

4. Conclusions

A 2D analytical model with polarization effect for the channel potential and the electric field distribution of the gate FP-HEMT in terms of Poisson's solution is reported. Weighting approach is used to consider the lateral spread of the depletion region between the FP and the drain. The relationships between our device model and drain bias, polarization effect, device structure parameters as well as AlGaN/GaN material parameters are discussed in detail. The approach to designing high breakdown voltage FP-HEMTs is also presented. The numerical simulation results verify the correctness of the proposed model. The model will be helpful for the designers to form accurate first-order design scheme and it presents an effective way to improve the breakdown performance of the FP-HEMTs. More importantly, the method can be employed to conveniently develop other analytical models for different device structures, such as MIS-HEMTs, multiple-FP HETMs, slant-FP HEMTs, etc.

References

[1] Conti F and Conti M 1972 *Solid-State Electron.* **15** 93
[2] Zhang N Q, Keller S, Parish G, Heikman S, DenBaars S P and Mishra U K 2000 *IEEE Electron Dev. Lett.* **21** 421
[3] Wu Y F, Saxler A, Moore M, Smith R P, Sheppard S, Chavarkar P M, Wisleder T, Mishra U K and Parikh P 2004 *IEEE Electron Dev. Lett.* **25** 117
[4] Peng M Z, Zheng Y K, Luo W J and Liu X Y 2011 *Solid-State Electron.* **64** 63
[5] Karmalkar S and Mishra U K 2001 *Solid-State Electron.* **45** 1645
[6] Koudymov A, Adivarahan V, Yang J, Simin G and Asif Khan M 2005 *IEEE Electron Dev. Lett.* **26** 704
[7] Horio K, Itagaki K and Nakajima A 2008 *International Conference on Microwave and Millimeter Wave Technology*, Nanjing, China
[8] Brannick A, Zakhleniuk N A, Ridley B K, Shealy J R, Schaff W J and Eastman L F 2009 *IEEE Electron Dev. Lett.* **30** 436
[9] Joh J and del Alamo J A 2006 *IEEE International Electron Devices Meeting*, San Francisco, CA, USA
[10] Joh J and del Alamo J A 2008 *IEEE Electron Dev. Lett.* **29** 287
[11] Karmalkar S, Shur M S, Simin G and Asif Khan M 2005 *IEEE Trans. Electron Dev.* **52** 2534
[12] Karmalkar S and Soudabi N 2006 *IEEE Trans. Electron Dev.* **53** 2430
[13] Xing H L, Dora Y, Chini A, Heikman S, Keller S and Mishra U K 2004 *IEEE Electron Dev. Lett.* **25** 161
[14] Dora Y, Chakraborty A, McCarthy L, Keller S, DenBaars S P and Mishra U K 2006 *IEEE Electron Dev. Lett.* **27** 713
[15] Pei Y, Chen Z, Brown D, Keller S, Denbaars S P and Mishra U K 2009 *IEEE Electron Dev. Lett.* **30** 328
[16] Kumar S P, Agrawal A, Chaujar R, Kabra S, Gupta M and Gupta R S 2007 *Microelectronics J.* **38** 1013
[17] Kumar S P, Agrawal A, Chaujar R, Gupta M and Gupta R S 2008 *Superlatt. Microstruc.* **44** 37
[18] Kumar S P, Agrawal A, Chaujar R, Gupta M and Gupta R S 2008 *Microelectronics J.* **39** 1416
[19] *ATLAS Device Simulator*, Santa Clara, CA: SILVACO Int. 2010
[20] Karmalkar S and Mishra U K 2001 *IEEE Trans. Electron Dev.* **48** 1515
[21] Shealy J R, Prunty T R, Chumbes E M and Ridley B K 2003 *J. Cryst. Growth* **250** 7
[22] Chung S K 2004 *IEE Proceedings Science, Measurement & Technology* **151** 21
[23] Anwar A F M and Faraclas E W 2006 *Solid-State Electron.* **50** 1041
[24] Ambacher O, Foutz B, Smart J, Shealy J R, Weimann N G, Chu K, Murphy M, Sierakowski A J, Schaff W J, Eastman L F, Dimitrov R, Mitchell A and Stutzmann M 2000 *J. Appl. Phys.* **87** 334
[25] Piprek J 2007 *Nitride Semiconductor Devices: Principles and Simulation* (Weinheim: Wiley-VCH).
[26] Mao W, Yang C, Hao Y, Ma X H, Wang C, Zhang J C, Liu H X, Bi Z W, Xu S R, Yang L A, Yang L, Zhang K, Zhang N Q and Pei Y 2011 *Chin. Phys. B* **20** 097203
[27] Saito W, Kuraguchi M, Takada Y, Tsuda K, Omura I and Ogura T *IEEE Trans. Electron Dev.* **52** 106
[28] Cao Y, Zimmermann T, Xing H L and Jena D 2010 *Appl. Phys. Lett.* **96** 042102